

Low-latitude magnetic flux emergence on rapidly rotating solar-type stars

EMRE IŞIK ¹, SAMI K. SOLANKI ¹, ROBERT H. CAMERON ¹ AND ALEXANDER I. SHAPIRO ¹

¹*Max-Planck-Institut für Sonnensystemforschung
Justus-von-Liebig-Weg 3, 37077 Göttingen, Germany*

ABSTRACT

Besides a dense coverage of their high latitudes by starspots, rapidly rotating cool stars also display low-latitude spots in Doppler images, although generally with a lower coverage. In contrast, flux emergence models of fast-rotating stars predict strong poleward deflection of radially rising magnetic flux as the Coriolis effect dominates over buoyancy, leaving a spot-free band around the equator. To resolve this discrepancy, we consider a flux tube near the base of the convection zone in a solar-type star rotating eight times faster than the Sun, assuming field intensification by weak-tube explosions. For the intensification to continue into the buoyancy-dominated regime, the upper convection zone must have a significantly steeper temperature gradient than in the Sun, by a factor that is comparable with that found in 3D simulations of rotating convection. Within the hypothesis that stellar active regions stem from the base of the convection zone, flux emergence between 1-20 degree latitudes requires highly supercritical field strengths of up to 500 kG in rapidly rotating stars. These field strengths require explosions of 100-kG tubes within the convection zone, compatible with reasonable values of the superadiabatic temperature gradient associated with the more rapid rotation.

Keywords: G dwarf stars(556) — Starspots (1572) — Stellar activity(1580) — Stellar magnetic fields (1610) — Solar analogs(1941) — Solar magnetic flux emergence (2000)

1. INTRODUCTION

Photospheres of cool stars with rotation periods of up to a few days are dominated by high-latitude or polar darkenings associated with magnetic flux concentrations (Strassmeier 2009). Unseen on the Sun, this is interpreted as the result of a combination of two effects that, in principle, can work in parallel. Firstly, at a sufficient rotation rate, the Coriolis acceleration experienced by rising flux tubes can overcome the radially outward directed acceleration caused by buoyancy (Schüssler & Solanki 1992). Secondly, at a sufficient emergence frequency, trailing-polarity flux from tilted bipolar magnetic regions emerging at any latitude diffuse and accumulate around polar regions. For very high levels of magnetic flux emergence, which lead to high activity levels, this accumulated flux is expected to form dark polar features (Schrijver & Title 2001) with enhanced lifetimes (Işık et al. 2007), or mixed-polarity polar spots

if the meridional flow is much faster than on the Sun (Holzwarth et al. 2006).

In spite of the apparent success of models reproducing starspots at high latitudes and poles of rapid rotators, numerical simulations of flux emergence all predict a ‘zone of avoidance’ between about $\pm 20^\circ$ latitudes, where no flux emergence occurs (Schüssler et al. 1996; Granzer et al. 2000; Işık et al. 2011, 2018). However, Doppler and Zeeman-Doppler imaging (hereafter DI and ZDI, respectively) reconstructions of rapidly rotating cool stars show occasional low-latitude spots (e.g., Rice & Strassmeier 2001; Jeffers et al. 2002; Perugini et al. 2021; Willamo et al. 2022). It is known that the resolving power of Doppler imaging is rather low in latitude. In addition, there is a possible information leak from mid-latitude activity on the less visible rotational hemisphere, depending on the axial inclination (Şenavcı et al. 2021). Nevertheless, low-latitude magnetic features are seen in most (Z)DI reconstructions of fast rotators, even though the latitude profile of the longitudinally averaged spot occupancy sharply drops equatorward of $\sim 20^\circ$ latitude in most cases.

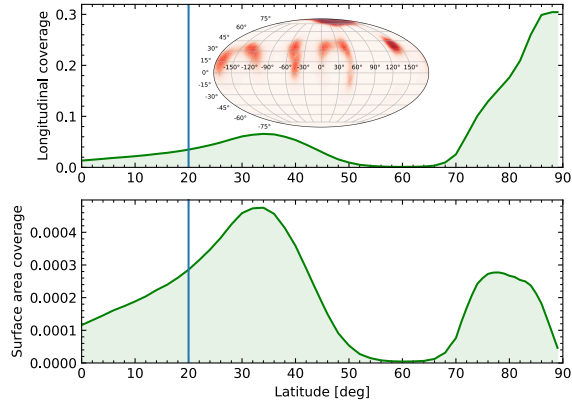


Figure 1. The latitudinal profile of longitude-averaged latitude occurrence (top panel) and the surface fraction of spots per degree of latitude on EK Dra in July 2015. The inset shows the surface reconstruction of spot filling factor with Doppler imaging. Note that the stellar inclination is 63° , so that no spots are visible on one rotational hemisphere. The image data was taken from Şenavcı et al. (2021).

An example latitude distribution is shown in Fig. 1, using data from Şenavcı et al. (2021). The latitudinal profile of relative spot occupancy is averaged over longitude, using the Doppler image reconstructed from a 15-night observing campaign. The top panel shows the latitude occurrence of spotted pixels on the map. The bottom panel shows the surface area per degree of latitude, which is covered by spot pixels, normalised to the surface area of the star. While there is a near-polar spot region spanning $70\text{--}90^\circ$ latitudes, the mid-latitude spots peak around 33° , with an elevated tail towards the equator. Spots below 20° -latitude are visible in the surface reconstruction (inset image). Note that low-latitude features with cross-equatorial extensions are likely artefacts of mid-latitude activity on the less visible rotational hemisphere (Şenavcı et al. 2021). Nonetheless, a number of the low-latitude spots are likely real. A theoretical picture of how such low-latitude features form amid rapid rotation is not yet available.

On the Sun, low-latitude flux emergence has important effects on the cross-equatorial transport of active-region dipole moments and hence for the build-up and long-term fluctuations of the global axial dipole moment (Cameron et al. 2013). Active regions emerging near the equator of a rapidly rotating active star can also drive a solar-like dipolar dynamo mode.

The photospheric magnetic field of the Sun is known to be far from uniform. It consists of a hierarchy of flux tubes that are organised into spots, pores, and smaller-scale concentrations (Solanki et al. 2006). Sunspot groups emerge as a consequence of the rise of bundles of magnetic flux from the solar convection zone (hereafter

CZ) (Weber et al. 2023). One model that reproduces several important characteristics of flux emergence on scales of sunspot groups makes use of numerical solutions of thin-flux-tube equations of ideal MHD. The model considers a toroidal ring that carries a similar magnetic flux as large solar active regions located near the base of the CZ. There the stratification is expected to be sufficiently sub-adiabatic to allow for mechanical equilibria in the presence of an internal flow along the tube axis. The tube has a sufficiently small cross section in comparison to the local pressure scale height (over which the thermodynamic quantities undergo significant changes). Linear stability analysis (Ferriz-Mas & Schüssler 1995) helped develop numerical models of flux-tube dynamics spanning the CZ (Caligari et al. 1995), which led to a series of results that are consistent with the observed trends of morphological and geometric properties of sunspot groups. For higher rotation rates and deeper convection zones (i.e., for lower Rossby numbers), the dynamical flux-tube simulations turned out to be consistent with the observation that mean latitudes of starspots are higher than on the Sun. However, when the initial flux-tube field strengths were taken following the approach in solar simulations (i.e., slightly above the onset of buoyancy instability that carries a flux tube to the surface), the resulting emergence patterns failed to reproduce low-latitude spots observed on fast rotators.

One poorly understood aspect is the depth of the original flux ring that gives rise to the eruption of a flux loop. To date, there has not been any conclusive result for the origin of the emerging flux loops on the Sun. Linear stability constraints hint towards the stably stratified lower part of the CZ as the seat of the flux tubes producing active-regions (Fan 2021). However, 3D simulations of magnetoconvection in a convective shell rotating three times faster than the Sun led to the formation of toroidal wreaths amid turbulent convective flows (Nelson et al. 2011, 2014). This result is consistent with a distributed dynamo, in which active-region producing flux tubes stem from a wide range of depths in the CZ. On the one hand, these simulations include much detail and insight into the physics of flux storage and emergence. On the other hand, the Reynolds number reached in such simulations is still far below that present within a stellar CZ. Furthermore, a subadiabatic lower convection zone (i.e., connecting to a radiative zone), which would facilitate flux storage also near the base, was not included in these models. However, it is relatively easier to provide statistics of flux emergence patterns with hundreds of thin flux tube simulations having different initial conditions (latitudes, field strengths, depths), considering the main bulk forces acting on any rising flux concentration in 3D

with a super-equipartition field. This approach is currently useful for modelling stellar magnetic activity with increasing rotation rate, until more realistic 3D magnetoconvection simulations for different rotation rates will become available.

We therefore study the intensification and breakup of thin toroidal flux tubes at the base of the CZ, at a rotation rate of eight times the solar rate ($P_{\text{rot}} = 3.125$ d), firstly by assuming a solar-like internal stratification based on non-local mixing-length theory, followed by a modified stratification adapted for the case of rapid rotation. Because the dynamo-generated magnetic flux in rapidly rotating stars is expected to be higher than on the Sun (as suggested by the empirical rotation-activity relation), it is conceivable that the flux density at the source depth can also reach higher levels of supercriticality than the near-critical levels for buoyancy instability. Can supercritical flux tubes form in the first place, and how?

We begin by considering a flux tube that is about 30 Mm above the base of the CZ, where the stratification turns from subadiabatic (entropy increasing outward) at the lower CZ to superadiabatic above. Here, the critical field strength for magnetic buoyancy instability is on the order of equipartition fields (10^4 G). When such a tube develops a loop that rises isentropically, the internal gas pressure at its apex will fall slower than the ambient pressure, until when the lateral pressure balance can be satisfied only if $B \rightarrow 0$, so the tube explodes (Moreno-Insertis et al. 1995; Rempel & Schüssler 2001; Hotta et al. 2012). Following drainage of material out of the exploded part, the cross-sectional area of such a tube will shrink along its sunken parts in the overshoot region, with a corresponding increase in magnetic field strength, on a time scale t_f which is short compared to the local timescale of the buoyant instability t_g . As the field becomes stronger, t_g changes faster than t_f , and at some critical field strength $t_f = t_g$ holds and the magnetic buoyancy instability becomes the dominant process, in the sense that the flux escapes faster than it is produced. We note that t_f depends on the superadiabaticity (the difference of the logarithmic temperature gradient from the corresponding adiabatic gradient) in the bulk of the convection zone and this is thought to be dependent on the rotation rate (Sect. 2.2). We therefore argue that the initial conditions for the flux tube simulations should depend on the stellar rotation rate. With plausible values of the field strength and the superadiabaticity, we find that flux loops producing starspot groups can (i) originate from the base of the CZ and (ii) lead to low-latitude emergence even for rapidly rotating stars.

In this study, we investigate the physical ranges of the field strength that can be reached, using the flux tube intensification mechanism outlined above (Sect. 2.2). Taking the resulting constraints into account, we place toroidal flux tubes at different depths in the overshoot layer below the convection zone of a star rotating at eight times the solar rate at the constrained range of field strengths. We study the effects of varying the initial depth and field strength in Sect. 3.1. Following that, we investigate the effect of the field strength for various internal differential rotation profiles and amplitudes in Sect. 3.2. We provide mapped probability distributions of latitude for the emerging flux, in Sect. 3.3. Discussing implications of our model in Sect. 4, we summarise our conclusions in Sect. 5.

2. FIELD INTENSIFICATION IN A FAST ROTATOR

2.1. The flux-tube model

We set up a toroidal flux tube with cross-sectional radius of R_t , located in a 1D non-local mixing-length model of the solar convection zone, using the thin-flux-tube approach (see Işık 2015, for details). Up to about $0.77R_{\odot}$, the stratification is subadiabatic (ie, locally stable to convective instability), but convective heat flux remains upward, driven by non-locally determined convective heat flux (Skaley & Stix 1991). At about $0.73R_{\odot}$, the convective heat flux changes sign (defined as the base of the CZ, at a radial location $r = r_b$), where the model allows for an overshoot region that extends the base of the CZ to about 10 Mm depth into the radiative interior. In the standard case, the stellar rotation is assumed to have the same differential rotation magnitude ($\Delta\Omega$) as in the Sun, but an equatorial rotation rate 8 times faster ($P_{\text{rot}} = 3.125$ d; we discuss the effect of differential rotation in Sect. 3.2). Following Ferriz-Mas & Schüssler (1995), we apply the linear stability analysis of a thin flux tube with a field strength B_0 in mechanical equilibrium, placed at a given initial depth $d_0 = r_b - r$ and latitude λ_0 . This gives the critical field strength $B_{\text{cr}}(d_0, \lambda_0)$, above which ‘supercritical’ flux tubes become unstable to first-order perturbations. In addition, the characteristic (e-folding) growth time t_g of the instability is calculated for $B_0 > B_{\text{cr}}(\lambda_0)$, i.e., for supercritical field strengths at a given latitude.

We let the initial field strengths be determined by contours of constant t_g on the (B_0, λ_0) plane at a given d_0 . Taking the initial condition to be mechanical equilibrium, we follow the nonlinear dynamics of flux tubes in 3D, using the Lagrangian code of Caligari et al. (1995), to track their peaks as they rise to the surface. The code solves the dynamics of a flux ring in ideal MHD,

under the effects of body forces (buoyancy, Lorentz, and hydrodynamic drag) and rotational forces, acting on 10^3 individual mass elements of the tube in their co-moving frame, from the overshoot region up to the subsurface ($\sim 0.98-0.99R_\star$), where the cross-sectional radius of the tube becomes of the order of the pressure scale height, making the thin flux tube approximation inapplicable. The simulations also take into account the differential rotation of the stellar convection zone (see Sect. 3.2 for more details on the internal rotation profiles considered).

2.2. Flux tube explosions in fast rotators

Prior to numerical simulations leading to low-latitude emergence, we estimate constraints on B_0 in a fast-rotating solar-type star, by considering possible effects of flux intensification and the convection-zone stratification. We assume that flux tubes are formed on a timescale t_f out of a mean toroidal field, which is wound up from a poloidal field by differential rotation throughout the convection zone. We put a conservative requirement that tubes must reach such field strengths sufficiently rapidly at a timescale $t_f \lesssim t_g$ before the magnetic buoyancy instability lifts them off the overshoot region into the convection zone. This is a conservative constraint in the sense that the actual time from the initial perturbation to the escape of a substantial amount of flux from the overshoot region is longer than t_g , as will be shown in Sect. 3.1.

To evaluate t_f , we consider a mechanism to form strong flux tubes at the base of the CZ, suggested by Rempel & Schüssler (2001). It exploits the potential energy available in the stratification of the CZ. Consider a tube with B_0 on the order of the equipartition value (10^4 G) and with sufficiently low flux Φ_0 , so that drag-braking during the rise would help hydrostatic equilibrium to be sustained along the tube. When the tube rises isentropically, its apex reaches a critical height in the CZ, where the internal gas pressure becomes equal to the external hydrostatic pressure, leading to $B \rightarrow 0$ and thus an explosion of that part of the tube (Moreno-Insertis et al. 1995). In the deeply buried horizontal parts, however, the field is amplified on the Alfvénic time scale, owing to draining of plasma out of the exploded part. The relevant time scale estimated by Rempel & Schüssler (2001) for the base of the solar CZ reads

$$t_f \simeq (\beta_0/C)^{1/2}, \quad (1)$$

where β_0 is the plasma beta (associated with the field strength of the original flux ring) and $C = 5 \times 10^7 \text{ yr}^{-2}$ is a constant, determined by the sound speed at the base of the CZ.

The scaling in Eq. (1) for the amplification time $\tau := t_f$ as a function of B_0 is indicated in Fig. 2 by the

black curve. In the solar convection zone, the explosion mechanism can work for magnetic fluxes on the order of 10^{17} Mx and for fields of up to a few times 10^4 G. The reason is that the explosion height r_e increases with the initial field strength of the tube, approximately following

$$r_e = r_0 + H_0 \left(\frac{\beta_0 \delta_s}{2} \right)^{-1/2}, \quad (2)$$

where H_0 is the pressure scale height at the initial location ($r = r_0$) and $\delta_s > 0$ is the mean superadiabaticity ($\delta(r) := \nabla(r) - \nabla_{\text{ad}}$) in the unstably stratified part of the convection zone, which is assumed to be constant in this basic estimation (Moreno-Insertis et al. 1995). Concerning field intensification, an explosion at r_e given by Eq. (2) can only make sense if $r_e < R_\odot$. Since the right-hand side is proportional to $B_0 \delta_s^{-1/2}$, the main factors determining the explosion radius are B_0 and δ_s . Assuming $\delta(r)$ to be the solar profile in our adopted stratification model, B_0 would then be strictly limited to $B_0 \lesssim 10^5$ G, to satisfy $r_e < R_\odot$. For stronger initial fields, the internal and external gas pressures do not match within the convection zone, so the tube reaches the surface, without leading to major intensification at its roots. For flux tubes starting at $d_0 = 5$ Mm and $\lambda_0 = 1^\circ$ in the Sun, the buoyancy instability sets in at $B_{\text{cr}} \sim 10^5$ G. Parker-unstable tubes that would carry sunspot-group fluxes have characteristic growth times $\tau := t_g$, following the orange curve in Fig. 2.

Increasing the rotation rate to $8\Omega_\odot$, tubes with $B_0 \simeq 10^5$ G become stable to perturbations at $d = 5$ Mm (except for friction-induced instability acting on $t \gg t_f$; Holzwarth 2008). B_{cr} and the corresponding B_0 range of unstable tubes with the same growth times are thus shifted to higher values, owing to the stabilising effect of rotation. The resulting range of B_0 for emerging flux tubes in $8\Omega_\odot$ is thus well beyond the range permitted by the $r_e < R_\star$ criterion of the explosion mechanism. Though the radius estimate in Eq. (2) is based on simple approximations, we confirmed it by a set of numerical simulations, where explosions took place inside the CZ only if $B_0 < 10^5$ (and for $\Phi_0 \lesssim 10^{18}$ Mx).

We assumed in the above discussion that δ_s in Eq. (2) does not change with Ω_\star . However, stars rotating faster than the Sun are expected to have more superadiabatic outer CZs, i.e., they have less efficient convection than in the Sun (Käpylä et al. 2005; Barker et al. 2014; Augustson & Mathis 2019). In simulations by Käpylä et al. (2005), the effects of rotation and convection are quantified by the Coriolis number, $\text{Co} = 2\Omega\tau_c$, where τ_c is the convective turnover time. For instance, a ten-fold change from $\text{Co}=1$ to $\text{Co}=10$ (equivalent to a ten-fold increase in Ω at a constant τ_c) raises δ_s by a factor of 3

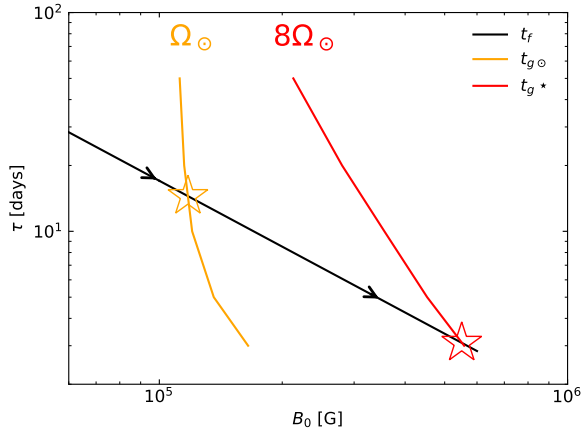


Figure 2. The intensification time t_f as a function of the initial field strength inside a flux tube according to Eq. (1), compared to the linear instability growth time t_g of magnetic flux tubes initially located at 5 Mm below the base of the convection zone at a latitude of 1° , in a star rotating at Ω_\odot (orange) and $8\Omega_\odot$ (red and other colours). As B_0 increases along the t_f curve with flux-tube explosions, the tubes are expected to become unstable and rise to the surface around field strengths marked by star symbols.

in the bulk of the upper CZ (see their Fig. 5). Eq. (2) would then indicate a decrease in the explosion radius r_e with increasing Ω_\star . We tested this effect, by modifying the surface temperature to be by 50-100 K cooler with a smooth transition from the interior, and calculated the resulting changes in pressure, density, and $\delta(r)$ (Rempel 2003; Işık 2015), resulting in an increase of δ_s by a factor of 3-10 in the upper CZ. Simulations using that modified stratification have led flux tubes with $B_0 = 7 - 10 \times 10^4$ G to explode between $0.95 - 0.97R_\star$.

Following an explosion at the tube apex, the field strength in the overshoot region can be amplified (on timescale t_f) by a factor of 3-5 in the 2D flux-sheet modelled by Rempel & Schüssler (2001), depending on the initial field strength. In 3D simulations, Hotta et al. (2012) found a factor of 2-3. When a 10^5 -G tube explodes at its apex in a fast rotator, its roots can thus be amplified towards the B_0 values required for the buoyancy instability (Fig. 2).

Although uncertainties remain for the internal stratification (Hotta et al. 2022), we consider the possibility that an enhanced superadiabaticity in the mid- to upper CZ of rapidly rotating CZs can make the field-amplification curve in Fig. 2 a viable path towards 500-kG fields near the base of the CZ of a star rotating at $8\Omega_\odot$, if the tube is amplified mainly by the non-local explosion mechanism. Downward pumping of magnetic flux driven by a turbulent diffusivity gradient is also a

possible pathway contributing to formation of intense magnetic flux tubes (e.g., Barker et al. 2012).

Consider a flux tube located at $d_0 = 5$ Mm in a solar-type star with $8\Omega_\odot$ being intensified up to a few times 10^5 G by flux-tube explosions. If $B_0 \lesssim 500$ kG, the tube can develop buoyancy instability at the timescale $t_g(B_0) > t_f(B_0)$ (the red curve in Fig. 2), when explosions are no longer possible. The condition $t_g \sim t_f$ (red star symbol in Fig. 2) puts another upper limit on the field strength that can be reached by flux-tube explosions on this fast rotator, because for $t_g \lesssim t_f$, the flux will be rapidly lost from the layer. The magnitude of this limit is comparable to the one implied by the explosion criterion $r_e < R_\star$ with $\delta_s(\Omega_\star)$ discussed above.

This comparison simply shows the expected mean behaviour and thus provides a crude estimate for the maximum field strength of flux tubes before they leave the region towards the surface. It is important to note that in the nonlinear dynamical simulations, the residence time of flux tubes in the overshoot region (Sect. 3.1) is considerably longer than the linear growth time of the instability. The latter timescale, t_g , only hints at the e-folding time of linear perturbations according to an analytical perturbation analysis. As long as the buoyant flux-loss criterion is concerned, field strengths between 500 to 600 kG would thus be possible to reach, provided that flux-tube explosions at $8\Omega_\odot$ can operate for stronger fields than on the Sun.

3. RESULTS

3.1. Dynamics of flux tubes near the equator

We carried out a series of simulations to compute the trajectory and shape of a thin flux tube in a parameter space spanned by the initial depth and field strength, as determined by the chosen t_g of the instability. The grid of initial parameters chosen are shown in Fig. 3. The curve for $d_0 = 5$ Mm is the same as the red curve in Fig. 2. The field strength at a given t_g increases with depth, because the ambient stratification becomes more subadiabatic, stabilising vertical displacements. As a result, the magnetic buoyancy needed to overcome this stabilising effect increases with depth. The resulting curves are still closely packed together, so that the intensification-emergence picture discussed in Sect. 2.2 is only weakly sensitive to the initial depth. The deepest case (9 Mm) is only 1000 km above the radiative zone (the radius of the flux tube we consider), where the temperature gradient becomes more or less constant with depth.

The radial location of the tube apex as a function of time is shown in Fig. 4, for a near-critical ($t_g = 20$ d) and a highly supercritical ($t_g = 3$ d) cases and various

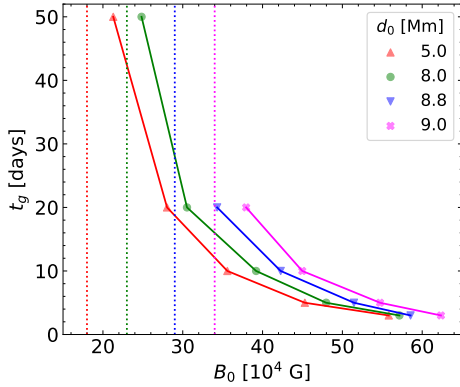


Figure 3. Characteristic growth time t_g for flux tubes in a star with $8\Omega_\odot$, located at depths d_0 below the base of the CZ. The vertical dotted lines show, with the respective colours, the onset field strengths of the buoyancy instability at each depth, i.e., with infinite linear growth time.

initial depths below the CZ-base ($5 < d_0 < 9$ Mm). The total rise time of the strongest flux tubes in our sample (i.e., with the shortest t_g of 3 days) is between 1-2 months from the initial perturbation to the emergence at the surface, leaving 1-2 weeks for the nonlinear development of the instability in the overshoot region (shown as a horizontal band). Although $t_g \simeq t_f$ (see Sect. 2.2), the duration of this nonlinear growth phase within the overshoot region is still longer than t_f by a factor of three, indicating that there is sufficient time for the intensification of the flux tube to a strength which allows for a nearly radial rise through the convection zone. For comparison, considering the weakest tubes with $t_g = 20$ d starting at $d_0 = 5$ Mm, the time it takes for a tube apex to leave the overshoot region is about six months.

The relation between the linear growth time and the full rise time is similar for different t_g values, i.e., initial field strengths. The deepest-located tubes with $d = 9$ Mm emerge earlier than most other cases. The reason for this irregular behaviour is the nonlinear dynamics (the interplay between various forces acting on each part of the tube), which amplify the resonant mode, leading to an early entry to the convection zone in some cases. In this particular case for 9 Mm, the buoyancy of the apex becomes large enough to trigger a fast rise before the restoring force acts for a sufficient time.

Figure 5 shows the emergence latitude as a function of the start latitude, the initial field strength, and the total rise time. Shown are simulations with two initial latitudes, namely 1 and 3 degrees. The apices of deeper-located and in particular stronger tubes are deflected poleward less strongly, owing to a stronger buoyancy and a faster rise. The emergence latitudes down to latitudes

$\lesssim 10^\circ$ are obtained, only in cases where the field strength is above 500 kG, which is about 5 times the critical field strength at the solar rotation rate, and about $2B_{\text{cr}}$ for the fast-rotator in consideration.

The emergence latitude is thus mainly sensitive to the field strength. As a secondary effect, the latitude is in general further decreased by 3-5 degrees with increasing depth at each constant growth rate, for fields above 300 kG, owing essentially to increased field strengths of tubes rooted at greater depth. The middle panel of Fig. 5 depicts how increasing magnetic buoyancy consistently brings the emergence latitudes from above 20 to below 10 degrees, while increasing the depth adds only a few more degrees. The functional dependence of B_0 on the linear growth rate t_g^{-1} of the instability is also depicted by the symbol size. The total rise time also indicates how long the Coriolis force can act on the rising tube (Fig. 5, right panel). Again, an increased magnetic buoyancy (B_0 marked by symbol size) leads to a faster rise, reducing the relative contribution of the Coriolis acceleration on the resulting rise trajectory.

Because the sensitivity of emergence latitudes on the initial depth is negligible when compared to that in the field strength, we confine the analysis in the rest of the study to a single depth ($d_0 = 5$ Mm), and vary t_g only.

3.2. Sensitivity to differential rotation

We employed two differential rotation profiles in this study. The first one is the cone-like rotation profile, which approximates the helioseismically inferred solar internal rotation:

$$\Omega(r, \lambda)/\Omega_{*,\text{eq}} = 1 + 2\frac{c_3}{\tilde{\omega}} - \left[1 + \text{erf}\left(\frac{r-r_0}{d}\right) \right] \times \frac{1}{\tilde{\omega}} (c_1 \sin^4 \lambda + c_2 \sin^2 \lambda + c_3), \quad (3)$$

where $\Omega_{*,\text{eq}}$ is the rotation rate at the equator, $\tilde{\omega}$ is the stellar equatorial rotation rate normalised to $\Omega_{\odot,\text{eq}}$, $c_1 = 0.0876$, $c_2 = 0.0535$, and $c_3 = 0.0182$ (Işık et al. 2018). The simulations in Sect. 3.1 were carried out under the rotation profile in Eq. (3).

As an alternative, we assume constant rotation along cylinders, to represent the Taylor-Proudman state of rotation, which is expected in very rapidly rotating stars (e.g. Lund et al. 2014):

$$\Omega(r, \lambda)/\Omega_{*,\text{eq}} = \begin{cases} \alpha + \Delta\Omega(r \cos \lambda) & \text{if } r > r_{\text{tach}} \\ \alpha + (\Delta\Omega)r_{\text{tach}} & \text{if } r < r_{\text{tach}}, \end{cases} \quad (4)$$

where $r_{\text{tach}} = 0.724R_\odot$, $\Delta\Omega$ is the pole-equator difference in angular velocity at the surface, set to the same value adopted in Eq. (3) as the solar reference value.

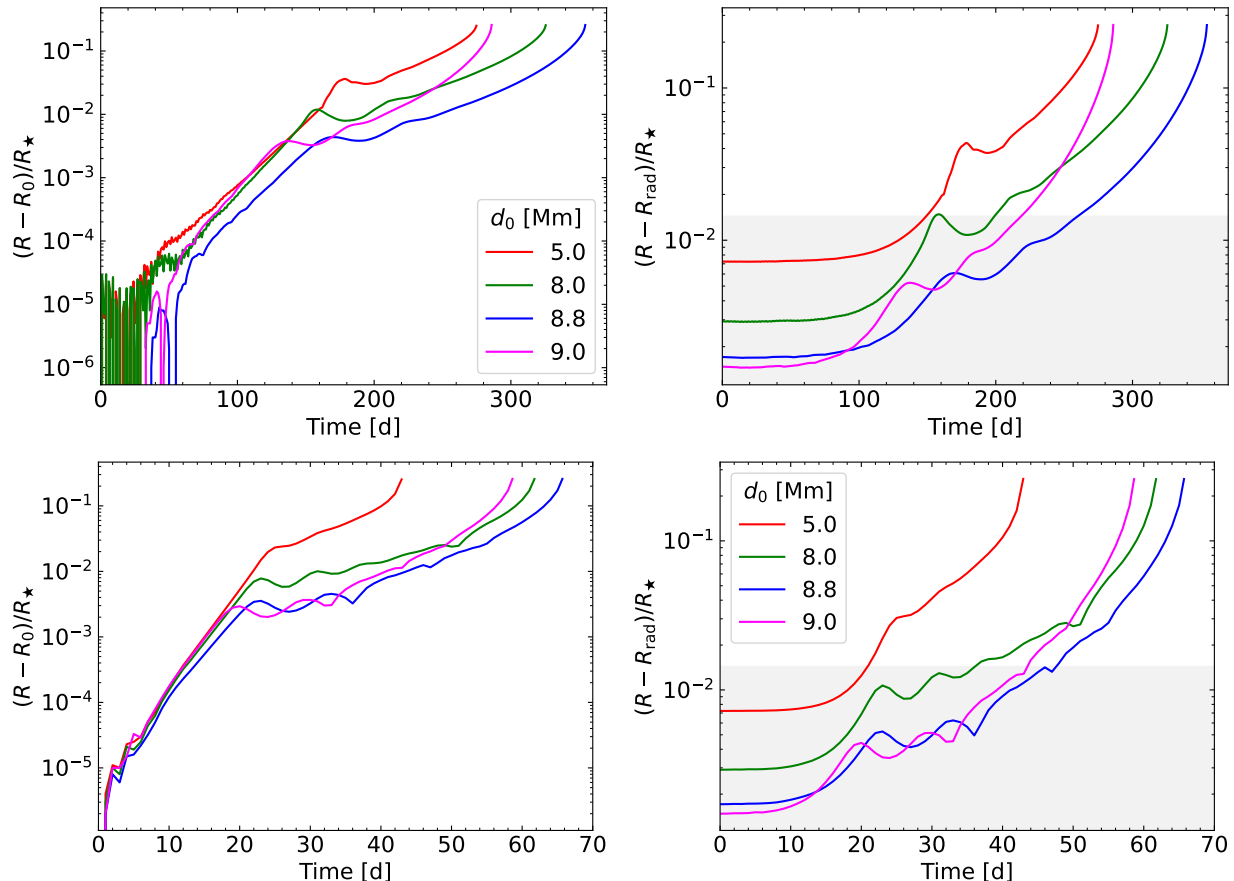


Figure 4. The radial displacement of the tube apex from the initial location R_0 (left panels) and relative to the base of the overshoot region (right panels) as a function of time, with different starting depths below the convection zone (colours), for a linear growth rate of 20 days (top panels) and 3 days (bottom panels). The grey horizontal band denotes the overshoot region.

The rotation profile for $8\Omega_\odot$ is expected to be closer to being cylindrical than to conical (Kitchatinov & Olemskoy 2012; Brun et al. 2022), so we adopt the profile Eq.(4) for simplicity, as modelling the detailed internal rotation for a given surface rotation rate is beyond the scope of the current study. Figure 6 shows the rotation contours for both idealised cases. As we show shortly, however, the rotation profile does not have a significant effect on the emergence latitude.

From observations, the surface shear is reported to be weakly increasing with $\tilde{\omega}$, following a power law $\Delta\Omega \propto \tilde{\omega}^p$, with the exponent ranging from 0.15 (Barnes et al. 2005) to 1.5 (Reiners 2006). We adopt $p = 0.20$ from the literature, which was found for G dwarfs, by interpolating over the effective temperature and the rotation rate of a stellar sample (Balona & Abedigamba 2016). As an extreme case, we also choose $p = 0.66$ following Messina & Guinan (2003), who estimated pole-equator lags from the photometrically observed range of rotational periods at a given star. These two choices for p corresponds to setting $\Delta\Omega$ in Eq. (4) to about 1.5 and 4 times the solar value.

A comparison of initial and emergence latitudes and the tilt angle distributions of flux tubes are given in Fig. 7 for rigid-body, solar-like, and cylindrical rotation laws (the latter for $p = 0.20$ and 0.66), with the initial depth $d_0 = 5$ Mm and linear growth time $t_g = 20$ d. The results are not very sensitive to the differential rotation profile except for somewhat smaller poleward deflections over a wide range of initial latitudes in the case $p = 0.66$. This justifies our use of solar-like rotation for the purposes of the earlier studies (Işık et al. 2011, 2018). The large tilt angle jumps in the solar-like rotation case were driven by the occurrence of two adjacent loops with different curvatures (Işık et al. 2018, Fig. 5). Such configurations do not form under the cylindrical rotation profile and the resulting tilt angle dependencies are relatively smooth.

The results of flux-tube rise simulations for various initial field strengths and the two shear amplitudes (for $p = 0.20$ and $p = 0.66$) are presented in Fig. 8. Poleward deflection of flux tubes is much suppressed by buoyancy in the case of short growth times (greater initial field strengths), leading to almost radial rise for the shortest

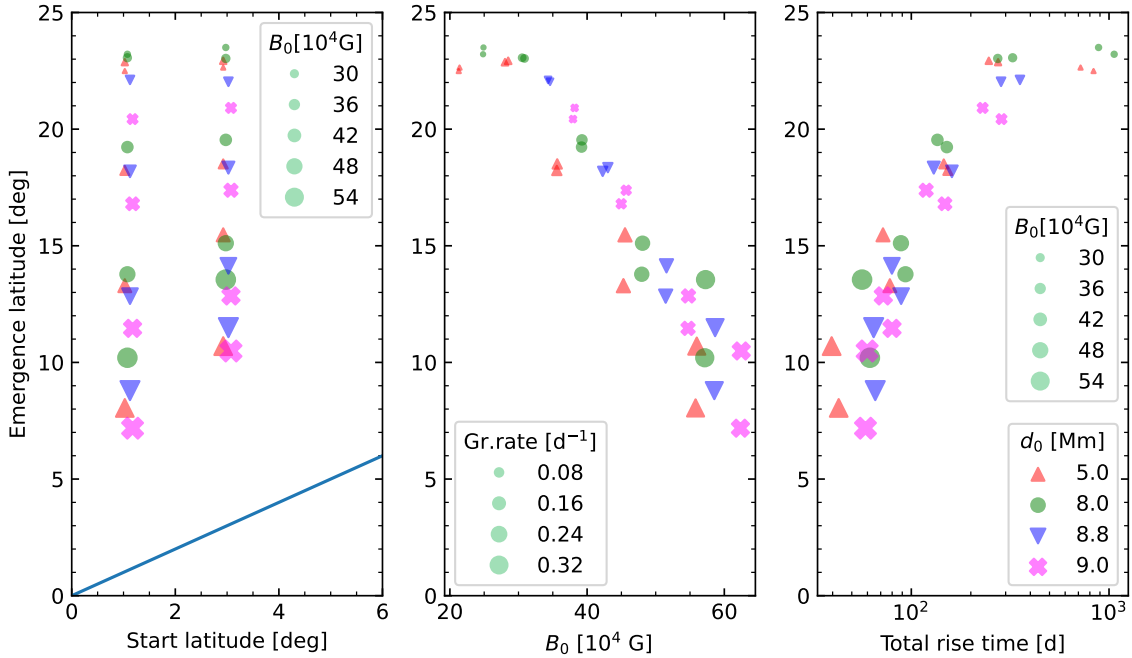


Figure 5. Emergence latitudes of flux tubes as a function of the initial latitude, field strength, and the total rise time (from the beginning of the initial perturbation). On each panel, the marker styles denote the initial depths as in Fig. 2. The symbol size shows the initial field strength on the left and right panels, and the linear growth rate on the middle panel. The blue line shows the radial-rise relation.

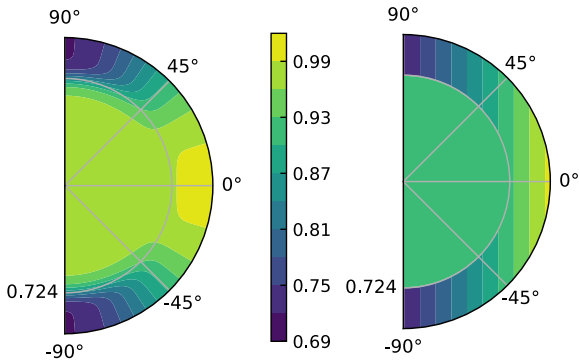


Figure 6. Contours of angular velocity normalised to the maximum at the equator at $r = 1$, for solar-like (left panel) and cylindrical (right panel) rotation profiles.

growth times. The emergence latitude is rather insensitive to the change in the differential rotation amplitude (from 1.5 to 4 times the solar value), whereas the tilt angles show an overall suppression by a few degrees.

3.3. Latitudinal distributions of emergence

Next, we investigate the main implications of highly supercritical flux tubes in shaping the latitudinal distribution of starspot emergence. To do so, we assumed three probability distribution functions (PDFs) for the

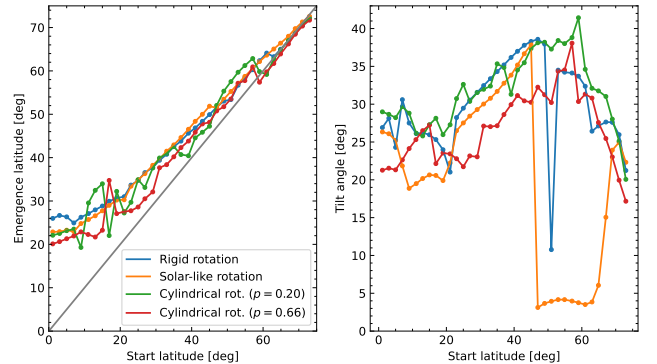


Figure 7. Emergence latitudes (left panel) and tilt angles (right panel) as a function of the initial latitude, at an initial depth of $d_0 = 5$ Mm below the base of the convection zone and $t_g = 20$ d. Note the relatively strong poleward deflection for low initial latitudes.

start latitudes of tubes at the base, and interpolate their nonlinear mapping to the surface, using the simulation results for $\tilde{\omega}_* = 8$ in Sect. 3.2 under the cylindrical rotation profile, Eq. (4), with the amplitude scaling exponent $p = 0.20$. The interpolation table spans initial latitudes from 1° to 73° and has an angular resolution of 2° . The upper limit of latitude is set by the linear instability boundary on the (B_0, λ_0) plane.

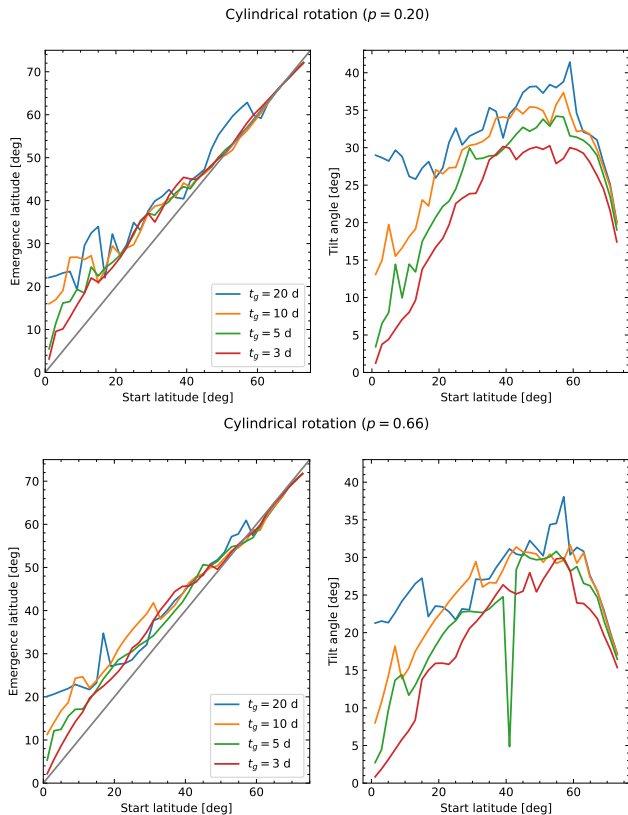


Figure 8. Similar to Fig. 7, for different initial magnetic field strengths corresponding to the indicated linear growth times, for $p = 0.20$ (top panel) and $p = 0.66$ (bottom panel).

We produce 10^4 random realisations, each following one of the uniform (between 1° and 70°), normal ($\mu = 40^\circ$, $\sigma = 12^\circ$), and triangular (peak at 40° in $(1^\circ, 70^\circ)$) PDFs for the start latitudes in the overshoot region, as shown on the top row of Fig. 9. We then interpolate the mappings in Fig. 8 for $p = 0.20$, to obtain the corresponding emergence latitude distributions, with an additive Gaussian noise in latitude, with $\sigma = 2^\circ$, to simulate possible effect of convective buffeting during the rise. When near-critical field strengths corresponding to $t_g = 20$ d are chosen, the emergence is confined above $\sim 20^\circ$ latitude (Fig. 9, middle row). For higher field strengths, the minimum latitude decreases, guided by the emergence latitudes in Fig. 8. For the shortest linear growth time that we consider (3 d; bottom panel), significant flux emerges between the equator and $\sim 20^\circ$ latitude. When the initial distributions are Gaussian or triangular, the fraction of emerging flux near the equator is less than for the uniform base distribution. These results hint at the possibility to estimate base distributions of toroidal flux using observed surface distributions, within a probabilistic inference framework that

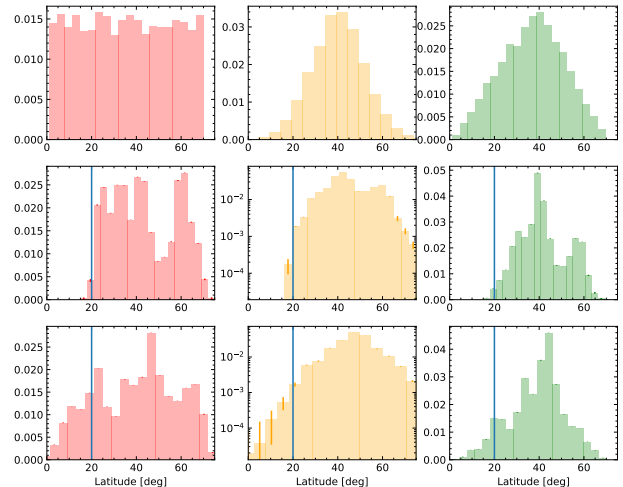


Figure 9. Normalised histograms for start latitudes at a depth of 5 Mm below the base of the convection zone (top panel; with uniform, normal, and triangular distributions), compared to emergence latitudes for near-critical ($t_d = 20$ d) and super-critical ($t_d = 3$ d) initial field strengths. The vertical lines are drawn for evaluating low-latitude emergence.

would also involve the surface flux transport layer of the FEAT model (Işık et al. 2018).

To test whether the substructure in the surface latitudinal distributions are not due to noise, we derived standard errors (σ/\sqrt{N}) from 20 independent realisations for each latitude bin (summing to 2×10^5 realisations per histogram). The resulting error bars are too small to be visible in most of the histogram bins. The multiple peaks in the surface distributions result from the non-uniform mapping between the base and the surface, making an inherent signature of the dynamics of flux rise on the surface. Such non-uniformities are also visible in some (azimuthally averaged) latitude distributions of active-star Doppler images similar to Fig. 1. However, the latter distributions are possibly contaminated by the low resolving power in latitude and possibly by the continuous redistribution of emerging flux on the stellar surface by horizontal transport processes.

4. DISCUSSION

In this study, we calculated the magnetic flux tube configurations which can give rise to low-latitude emergence of magnetic flux in a solar-like convection zone rotating eight times faster than the Sun ($P_{\text{rot,eq}} = 3.125$ days). To shift the lowest emergence latitude of flux tubes originating from the base of the convection zone from above $\sim 20^\circ$ to about 7° for solar-like conical shear, or 3° for cylindrical shear, our computations require field strengths that are stronger than the near-critical ($B \sim B_{\text{cr}}$) levels ($t_g = 20$ d) by a factor of about 2. The

same supercriticality factor is about 1.6 near the base of the overshoot region ($d_0 = 9$ Mm).

We studied two main effects that are likely to determine the initial field strength of flux tubes near the base of the convection zone. As the amplifying source, we considered explosions of flux tubes carrying significantly low flux in the superadiabatic part of the convection zone (see also [Weber et al. 2011](#), for the impact of convective flows on thin flux tubes). For this effect to be functional up to field strengths compatible with low-latitude emergence, we found that the bulk of the unstably stratified part of the convection zone must be more superadiabatic than in solar models, by a factor of about three, so that explosions of 10^5 -G tubes (with presumably lower fluxes than non-exploding ones) would be possible within the CZ. This requirement is consistent with the global MHD simulations of rotating convection, indicating a reduction in the efficacy of convection with increasing Coriolis number. In this way, low-latitude-emerging tubes with $B_0 = 500$ kG can be formed. The second important effect is the magnetic buoyancy instability, whose growth rate increases faster with the tube strength than the amplification rate (see Sect. 2.2, Fig. 2). Because the unstable flux tubes require considerably longer to break out of the overshoot layer than the linear growth-time constraint (Sect. 3.1), we expect the buoyancy constraint not to strongly impede the amplification process in the nonlinear regime, for $B_0 \lesssim 500$ kG.

Doppler images of rapidly rotating G-K stars often show low-latitude spot concentrations, but generally only a few at a given time, as opposed to much higher spot coverage at mid- to high latitudes. In the context of our results, we can interpret the observed latitudinal distribution of starspots as follows: starspot-producing flux tubes can form over a range of field strengths at various depths in the overshoot layer, with a given probability density of formation at a given field strength. Formation of exceptionally strong flux tubes have more radial rise trajectories than weaker ones. If the flux tube in the overshoot layer was ejected from near the equator, then this can lead to a low-latitude active region. The flux-rise mapping of the most buoyant tubes in our sample shows that even for a uniform base distribution (Fig. 9, bottom panel), the surface distribution declines towards the equator, consistent with Doppler imaging results.

The dynamo generation of toroidal flux and the surface patterns driven by flux emergence and surface transport are all likely to contribute to the observed patterns of surface activity ([Işık et al. 2011](#)). The surface manifestations of stellar activity will be partly determined by the distribution of toroidal flux in the convection zone,

from which starspot-producing flux loops would originate. Knowing the toroidal flux distribution requires better understanding of dynamos at various rotation rates (see, e.g., [Finley et al. 2024](#)). By taking toroidal flux distributions in the convection zone and accounting for low-latitude emergence of magnetic flux on stars rotating up to 10 times the solar rate, the distribution and evolution of starspots can be modelled, using surface flux transport models. The resulting surface maps can be used in forward-modelling observational diagnostics, in comparison with observations (e.g., [Sowmya et al. 2022](#); [Němec et al. 2023](#)).

In a recent study, [Zhang et al. \(2024\)](#) introduced a rotation-dependent mean latitude for the surface source of a flux-transport dynamo model, to find shorter activity cycles and a mode change of the global field from dipole to quadrupole as the rotation period decreases. Motivated by our results, we note that low-latitude emergence of active regions near the equator can have a constructive effect on the global dipole even for fast rotators, if the Coriolis-induced tilt angles of emerging bipoles or the random impact of convective motions are large enough ([Weber et al. 2023](#), and references therein). In the current study, we find a tilt angle of 3° for the minimum emergence latitude reached (7°) in the $d_0 = 9$ Mm case, and $1 - 5^\circ$ for the cylindrical-rotation cases and t_g of 3-5 days.

We have assumed that the magnetic flux that forms stellar active regions has its source near the base of the convection zone, where the stratification is sufficiently stable for super-equipartition (and super-critical) flux tubes to form. However, the thin flux tube model has several limitations. Relevant to the present context, (a) the flux emergence dynamics from the subsurface into the photosphere is out of its scope; (b) the sizes of solar active regions are smaller than what is predicted by the model, where the unstable loop has a considerably longer azimuthal extent (sunspot groups can also be fragments of larger-scale loops that form in the convection zone). Convective and rotational effects within that skin depth near the surface can also have substantial effects in the formation of solar and stellar active regions ([Weber et al. 2023](#), and the references therein). Although no studies have so far ruled out the possibility for sunspot groups to originate from the base of the convection zone, an alternative flux emergence mechanism can be led by a distributed dynamo ([Käpylä et al. 2023](#), and the references therein), where flux tubes can form in the midst of the convection zone, e.g., out of shear-generated wreaths and they can rise to the surface, subject to buoyancy and convective flows ([Nelson et al. 2011, 2014](#); [Weber et al. 2023](#)). In such convective

dynamo action, flux tubes starting from low latitudes not very far below the surface could emerge at low latitudes more easily, owing to the relative proximity of the source region to the surface.

5. CONCLUSION

We studied the storage, intensification, and rise properties of magnetic flux in a solar-type star rotating with a period of about 3 days, within the thin flux tube approximation. We find,

- The initial field strength required for the low-latitude emergence is about 500 kG. Flux tubes can be amplified to such strengths in a series of failed emergences (explosions) of weaker flux tubes, provided that the temperature gradient in the upper convection zone increases with the rotation rate.
- Field strengths of order 500 kG can be established inside flux tubes before they would be lost from the overshoot region.
- The suppression of poleward deflection is more sensitive to the field strength than to the depth at which a flux tube is located in the overshoot layer.

- The results have only a weak dependency on the detailed shape and amplitude of internal differential rotation.
- Various initial latitude distributions of flux tubes end up with similar emergence distributions, peaking around some latitudes and showing a tail towards the equator, similar to Doppler imaging observations.

Our results will have implications for the forward modeling of observational diagnostics of active stars (see [Işık et al. 2023](#), Sect. 3) and attempts to constrain stellar dynamo models (see [Charbonneau & Sokoloff 2023](#), Sect. 11). One consequence of taking into account low-latitude emergence in active stars would be a better estimation of the contribution of faculae to brightness variations in the rotational and activity-cycle time scales ([Němec et al. 2022](#)). Another implication would be in the forward modelling of chromospheric activity indices for active stars, which we plan to cover in an upcoming study.

Acknowledgments. We thank the anonymous reviewer whose critical comments helped us to improve the manuscript considerably. We acknowledge Hakan V. Şenavcı for providing the Doppler-imaging map of EK Dra in Fig. 1.

REFERENCES

- Augustson, K. C., & Mathis, S. 2019, *ApJ*, 874, 83, doi: [10.3847/1538-4357/ab0b3d](#)
- Balona, L. A., & Abedigamba, O. P. 2016, *MNRAS*, 461, 497, doi: [10.1093/mnras/stw1443](#)
- Barker, A. J., Dempsey, A. M., & Lithwick, Y. 2014, *ApJ*, 791, 13, doi: [10.1088/0004-637X/791/1/13](#)
- Barker, A. J., Silvers, L. J., Proctor, M. R. E., & Weiss, N. O. 2012, *MNRAS*, 424, 115, doi: [10.1111/j.1365-2966.2012.21174.x](#)
- Barnes, J. R., Collier Cameron, A., Donati, J. F., et al. 2005, *MNRAS*, 357, L1, doi: [10.1111/j.1745-3933.2005.08587.x](#)
- Brun, A. S., Strugarek, A., Noraz, Q., et al. 2022, *ApJ*, 926, 21, doi: [10.3847/1538-4357/ac469b](#)
- Caligari, P., Moreno-Insertis, F., & Schüssler, M. 1995, *ApJ*, 441, 886, doi: [10.1086/175410](#)
- Cameron, R. H., Dasi-Espuig, M., Jiang, J., et al. 2013, *A&A*, 557, A141, doi: [10.1051/0004-6361/201321981](#)
- Charbonneau, P., & Sokoloff, D. 2023, *SSRv*, 219, 35, doi: [10.1007/s11214-023-00980-0](#)
- Fan, Y. 2021, *Living Reviews in Solar Physics*, 18, 5, doi: [10.1007/s41116-021-00031-2](#)
- Ferriz-Mas, A., & Schüssler, M. 1995, *Geophysical and Astrophysical Fluid Dynamics*, 81, 233, doi: [10.1080/03091929508229066](#)
- Finley, A. J., Brun, A. S., Strugarek, A., & Cameron, R. 2024, *A&A*, 684, A92, doi: [10.1051/0004-6361/202347862](#)
- Granzer, T., Schüssler, M., Caligari, P., & Strassmeier, K. G. 2000, *A&A*, 355, 1087
- Holzwarth, V. 2008, *A&A*, 485, 351, doi: [10.1051/0004-6361:200809564](#)
- Holzwarth, V., Mackay, D. H., & Jardine, M. 2006, *MNRAS*, 369, 1703, doi: [10.1111/j.1365-2966.2006.10407.x](#)
- Hotta, H., Kusano, K., & Shimada, R. 2022, *ApJ*, 933, 199, doi: [10.3847/1538-4357/ac7395](#)
- Hotta, H., Rempel, M., & Yokoyama, T. 2012, *ApJL*, 759, L24, doi: [10.1088/2041-8205/759/1/L24](#)
- Işık, E. 2015, *ApJL*, 813, L13, doi: [10.1088/2041-8205/813/1/L13](#)

- Işık, E., Schmitt, D., & Schüssler, M. 2011, *A&A*, 528, A135, doi: [10.1051/0004-6361/201014501](https://doi.org/10.1051/0004-6361/201014501)
- Işık, E., Schüssler, M., & Solanki, S. K. 2007, *A&A*, 464, 1049, doi: [10.1051/0004-6361:20066623](https://doi.org/10.1051/0004-6361:20066623)
- Işık, E., Solanki, S. K., Krivova, N. A., & Shapiro, A. I. 2018, *A&A*, 620, A177, doi: [10.1051/0004-6361/201833393](https://doi.org/10.1051/0004-6361/201833393)
- Işık, E., van Saders, J. L., Reiners, A., & Metcalfe, T. S. 2023, *SSRv*, 219, 70, doi: [10.1007/s11214-023-01016-3](https://doi.org/10.1007/s11214-023-01016-3)
- Jeffers, S. V., Barnes, J. R., & Collier Cameron, A. 2002, *MNRAS*, 331, 666, doi: [10.1046/j.1365-8711.2002.05143.x](https://doi.org/10.1046/j.1365-8711.2002.05143.x)
- Käpylä, P. J., Browning, M. K., Brun, A. S., Guerrero, G., & Warnecke, J. 2023, *SSRv*, 219, 58, doi: [10.1007/s11214-023-01005-6](https://doi.org/10.1007/s11214-023-01005-6)
- Käpylä, P. J., Korpi, M. J., Stix, M., & Tuominen, I. 2005, *A&A*, 438, 403, doi: [10.1051/0004-6361:20042244](https://doi.org/10.1051/0004-6361:20042244)
- Kitchatinov, L. L., & Olemskoy, S. V. 2012, *MNRAS*, 423, 3344, doi: [10.1111/j.1365-2966.2012.21126.x](https://doi.org/10.1111/j.1365-2966.2012.21126.x)
- Lund, M. N., Miesch, M. S., & Christensen-Dalsgaard, J. 2014, *ApJ*, 790, 121, doi: [10.1088/0004-637X/790/2/121](https://doi.org/10.1088/0004-637X/790/2/121)
- Messina, S., & Guinan, E. F. 2003, *A&A*, 409, 1017, doi: [10.1051/0004-6361:20031161](https://doi.org/10.1051/0004-6361:20031161)
- Moreno-Insertis, F., Caligari, P., & Schuessler, M. 1995, *ApJ*, 452, 894, doi: [10.1086/176357](https://doi.org/10.1086/176357)
- Nelson, N. J., Brown, B. P., Brun, A. S., Miesch, M. S., & Toomre, J. 2011, *ApJL*, 739, L38, doi: [10.1088/2041-8205/739/2/L38](https://doi.org/10.1088/2041-8205/739/2/L38)
- Nelson, N. J., Brown, B. P., Sacha Brun, A., Miesch, M. S., & Toomre, J. 2014, *SoPh*, 289, 441, doi: [10.1007/s11207-012-0221-4](https://doi.org/10.1007/s11207-012-0221-4)
- Nèmec, N. E., Shapiro, A. I., Işık, E., Solanki, S. K., & Reinhold, T. 2023, *A&A*, 672, A138, doi: [10.1051/0004-6361/202244412](https://doi.org/10.1051/0004-6361/202244412)
- Nèmec, N. E., Shapiro, A. I., Işık, E., et al. 2022, *ApJL*, 934, L23, doi: [10.3847/2041-8213/ac8155](https://doi.org/10.3847/2041-8213/ac8155)
- Perugini, G. M., Marsden, S. C., Waite, I. A., et al. 2021, *MNRAS*, 508, 3304, doi: [10.1093/mnras/stab2711](https://doi.org/10.1093/mnras/stab2711)
- Reiners, A. 2006, *A&A*, 446, 267, doi: [10.1051/0004-6361:20053911](https://doi.org/10.1051/0004-6361:20053911)
- Rempel, M. 2003, *A&A*, 397, 1097, doi: [10.1051/0004-6361:20021594](https://doi.org/10.1051/0004-6361:20021594)
- Rempel, M., & Schüssler, M. 2001, *ApJL*, 552, L171, doi: [10.1086/320346](https://doi.org/10.1086/320346)
- Rice, J. B., & Strassmeier, K. G. 2001, *A&A*, 377, 264, doi: [10.1051/0004-6361:20011002](https://doi.org/10.1051/0004-6361:20011002)
- Schrijver, C. J., & Title, A. M. 2001, *ApJ*, 551, 1099, doi: [10.1086/320237](https://doi.org/10.1086/320237)
- Schüssler, M., Caligari, P., Ferriz-Mas, A., Solanki, S. K., & Stix, M. 1996, *A&A*, 314, 503
- Schüssler, M., & Solanki, S. K. 1992, *A&A*, 264, L13
- Şenavcı, H. V., Kılıçoğlu, T., Işık, E., et al. 2021, *MNRAS*, 502, 3343, doi: [10.1093/mnras/stab199](https://doi.org/10.1093/mnras/stab199)
- Skaley, D., & Stix, M. 1991, *A&A*, 241, 227
- Solanki, S. K., Inhester, B., & Schüssler, M. 2006, *Reports on Progress in Physics*, 69, 563, doi: [10.1088/0034-4885/69/3/R02](https://doi.org/10.1088/0034-4885/69/3/R02)
- Sowmya, K., Nèmec, N. E., Shapiro, A. I., et al. 2022, *ApJ*, 934, 146, doi: [10.3847/1538-4357/ac79b3](https://doi.org/10.3847/1538-4357/ac79b3)
- Strassmeier, K. G. 2009, *A&A Rv*, 17, 251, doi: [10.1007/s00159-009-0020-6](https://doi.org/10.1007/s00159-009-0020-6)
- Weber, M. A., Fan, Y., & Miesch, M. S. 2011, *ApJ*, 741, 11, doi: [10.1088/0004-637X/741/1/11](https://doi.org/10.1088/0004-637X/741/1/11)
- Weber, M. A., Schunker, H., Jouve, L., & Işık, E. 2023, *SSRv*, 219, 63, doi: [10.1007/s11214-023-01006-5](https://doi.org/10.1007/s11214-023-01006-5)
- Willamo, T., Lehtinen, J. J., Hackman, T., et al. 2022, *A&A*, 659, A71, doi: [10.1051/0004-6361/202141649](https://doi.org/10.1051/0004-6361/202141649)
- Zhang, Z., Jiang, J., & Kitchatinov, L. 2024, *A&A*, 686, A90, doi: [10.1051/0004-6361/202348201](https://doi.org/10.1051/0004-6361/202348201)